Cell Reports
Physical Science

CellPress
OPEN ACCESS

Article

Demonstrating stability within parallel connection as a basis for building large-scale battery systems

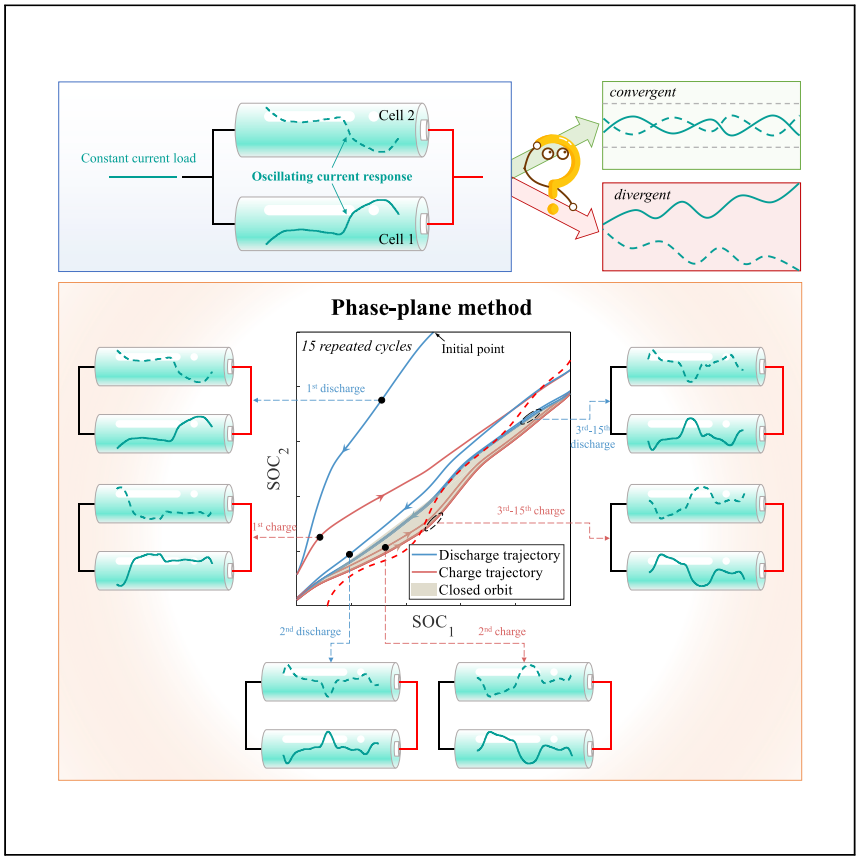

Parallel connection of cells is a fundamental configuration within large-scale battery energy storage systems. Here, Li et al. demonstrate systematic proof for the intrinsic safety of parallel configurations, providing theoretical support for the development of battery energy storage systems.

Zhe Li, Anhao Zuo, Zhaobin Mo, ..., Jianbo Zhang, Markus H. Hofmann, Andreas Jossen

zhe_li@tsinghua.edu.cn

Highlights

A parallel configuration of cells generates self-excited current oscillation

The parallel battery system is shown to be convergent, stable, and robust

Long-term trajectory in repeated cycles is enveloped in a closed orbit

Warnings are given about capacity loss, possible current overload, and malfunctions

Li et al., Cell Reports Physical Science 3, 101154
December 21, 2022
https://doi.org/10.1016/j.xcrp.2022.101154

Cell Reports
Physical Science

CellPress
OPEN ACCESS

Article

Demonstrating stability within parallel connection as a basis for building large-scale battery systems

Zhe Li,[1,4,*] Anhao Zuo,[1] Zhaobin Mo,[1] Mu Lin,[2] Chengyu Wang,[1] Jianbo Zhang,[1] Markus H. Hofmann,[3] and Andreas Jossen[3]

SUMMARY

Cells are often connected in parallel to achieve the required energy capacity of large-scale battery systems. However, the current on each branch could exhibit oscillation, thus causing concerns about current runaway or even system divergence. Here, we demonstrate that oscillation is self-excited even under a constant load owing to the inherent nonlinearity of the parallel configuration. By adopting a phase-plane method, we find that the currents of cells connected in parallel are at no risk of running away, and their trajectories approach a stable closed orbit in the phase-plane portrait after numerous repeated cycles of charging and discharging. This finding indicates that the parallel configuration is convergent and therefore safe, stable and therefore controllable, and initial-state independent and therefore robust. Although the parallel configuration proves to be convergent, stable, and robust, we also warn about inevitable capacity loss, possible current overload, and accidental malfunctions within parallel configurations.

INTRODUCTION

According to BP's primary energy share projections,[1] the proportion of renewable energy will increase to 65% by 2050, achieving a 95% reduction in carbon emissions in the *Net-Zero* scenario. The promising renewable energy is "a flash in the pan" without being supported by the continuing electrification of energy storage systems. It is estimated that 999 GWh of new energy storage capacity will be added worldwide between 2021 and 2030.[2] Series and parallel connections of batteries, the fundamental configurations of battery systems with any type of topology, enable large-scale battery energy storage systems (BESSs). Series connections help increase the system voltage, while parallel connections help increase the capacity. The number of series connections is limited by the electrical isolation equipment, the cost of power electronics,[3,4] and the balancing requirement. Because of this limitation, the number of parallel connections is increasing to improve energy use in a variety of systems. Each module of the Tesla Model S 85 kWh battery pack comprises six groups of 74 cells connected in parallel.[5] The world's largest BESS, the Red Sea Project, featuring 1,300 MWh of battery energy,[6] may have larger parallel groups. The number of parallel connections used in the large-scale BESS is unprecedented in human history. A widely concerned problem of the parallel configuration is the uneven distribution of current and state of charge (SOC) on different branches due to cell-to-cell variations on capacity,[7–13] resistance,[7,9,10,12–16] temperature,[7,11,13,16–20] and aging level.[21,22] Not only is the current of each branch distributed, but the current could exhibit oscillation,[16,20,23–28] causing concerns and speculations about

[1]State Key Laboratory of Automotive Safety and Energy, Tsinghua University, Beijing, China

[2]School of Statistics and Mathematics, Central University of Finance and Economics, Beijing, China

[3]Institute for Electrical Energy Storage Technology, Technical University of Munich, Munich, Germany

[4]Lead contact

*Correspondence: zhe_li@tsinghua.edu.cn

https://doi.org/10.1016/j.xcrp.2022.101154

current runaway or system divergence, that is, intrinsic hazards of the parallel configuration. More than 45 BESS-related accidents from 2017 to 2022 in South Korea, China, America, and Australia, among others, also prompt us to reconsider whether system failure is attributed to cell failure or an intrinsic hazard of the parallel configuration. However, the safety of parallel designs has been taken for granted to date by researchers and engineers, and the current on parallel branches in the battery management system is seldom monitored.[29] Therefore, despite its frequent appearance in plenty of literature, current oscillation has been rarely investigated in terms of its intrinsic stability.

In this study, based on a simple numerical experiment involving a two-cell parallel system, we demonstrate that the current oscillation results from the inherent nonlinearity of the parallel configuration. To make clear whether the oscillation could trigger failures, we adopt a phase-plane method to elucidate long-term behaviors during numerous repeated cycles of charging and discharging. We systematically prove that the currents of two cells connected in parallel are at no risk of running away, and their trajectories approach a stable closed orbit in the phase-plane portrait after numerous repeated cycles of charging and discharging. Many representative numerical experiments of two-cell parallel systems have verified the conclusions. We further generalize the conclusions to multi-cell parallel systems. This finding indicates that the parallel configuration is convergent and therefore safe, stable and therefore controllable, and initial-state independent and therefore robust. Nevertheless, we also warn about some risks behind stability. First, parallel battery systems inflict intrinsic capacity loss due to cell inconsistencies, causing capacity loss even reaching up to 34% according to the terminals of the closed orbit. Secondly, during the cell-balancing process, the current on a certain branch could be too large, thus causing possible current overload. Thirdly, the cell may be in a fixed state in particular usage scenarios. This study sheds light on the essential safety of parallel battery configurations, which lays a basis for the continued building of large-scale battery systems.

RESULTS AND DISCUSSION

Oscillation originating from inherent nonlinearity in parallel systems

Cell-to-cell variations of capacity, resistance, temperature, and aging levels can exactly explain the current distribution and subsequent SOC distribution through the integral of current but is inadequate for elucidating the oscillation of every single current appearing in a large number of experiments and simulations.[16,20,23–28] Most oscillations on each branch in the parallel circuits are low frequency (there are only a few waves during a full discharge) and present nonconstant wavelength, nonfixed amplitude, and nonstandard shape. Figure S1 gives an example.

For systems governed by linear equations such as one cell described by Rint model[30] with constant parameters, oscillating current during a full discharge always implies an oscillating input load, such as an oscillating voltage excitation. Notably, the Rint model describes the basic characteristics of the cell, and more complex high-order Resistor-Capacitor models just incorporate relaxation processes based on the Rint model.

For nonlinear systems, a constant load could lead to variable responses: steady or oscillating, periodic or random, convergent or divergent. Considering a two-cell parallel system, the ordinary differential equation (ODE) is shown in Note S1. Two major parameters in the ODE are open-circuit voltage (E) and internal resistance (R), which are the cell voltage without any external load and the opposition to the

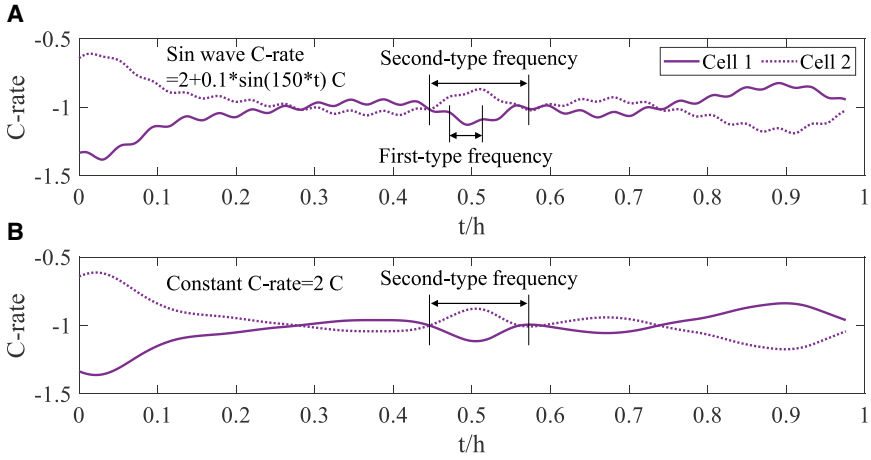

Figure 1. The second-type frequency remains unchanged in the current response in the parallel system

The current response on each branch was obtained by applying a sin-wave C-rate (A) or a constant C-rate (B) on the main circuit loop. Parameters are shown in Figure 3. The ODE of the two-cell parallel system in Note S1 was simulated by an ODE solver in MATLAB.

current flow within the cell, respectively. In practice, open-circuit voltage and internal resistance typically vary with SOC, material type, aging condition, and temperature. Therefore, the ODE is highly nonlinear due to the nonlinear variation of open-circuit voltage (E) and resistance (R), relative to cell SOC. For this nonlinear battery system with a parallel configuration, the current oscillation could be either the consequence of external excitation or the inherent property originating from system nonlinearity. A simple numerical experiment could help identify the trigger. Under the hypothesis of a sin-wave current load on the main circuit loop, there appear two frequencies in the current response (Figure 1A). The frequency of the first type follows that of the sin-wave load and disappears when the current load becomes constant (Figure 1B). At the same time, the second-type frequency cannot be eliminated even if the system load becomes constant, which reveals the inherent nonlinearity of the parallel configuration (Figure 1B).

Stability due to approach a stable closed orbit after cycles of charge and discharge

Confronting the disturbing oscillations originating from the system's intrinsic property, we have not made clear if they could trigger failures, such as divergence, instability, and poor robustness. Once these risks exist, the safety and controllability of battery systems will be seriously threatened.

Given obtaining an analytical solution of the nonlinear equations (Note S1) is almost impossible, we borrow the phase-plane method (Note S2) in nonlinear dynamics theory, which has been chiefly applied in studies of mechanical moving[31] and atmosphere motion[32] originally. The solutions over time of nonlinear equations (SOC_1, SOC_2) with an initial SOC value correspond to an SOC trajectory (blue curves in Figure 2A) in the phase-plane portrait of the parallel system. It is noteworthy that the parallel system only operates within a physically meaningful zone (PMZ) of $[0,1] \times [0,1]$ (Figure 2A), which is specifically a switched dynamical system. A simple instance with the same linear parameters is shown: with the initial value (1, 0), the cell SOC will move to (0.03, 0) along the violet trajectory (Figure 2A), and the temporal evolution of the corresponding SOC and current is shown in Figure 2B. The unique

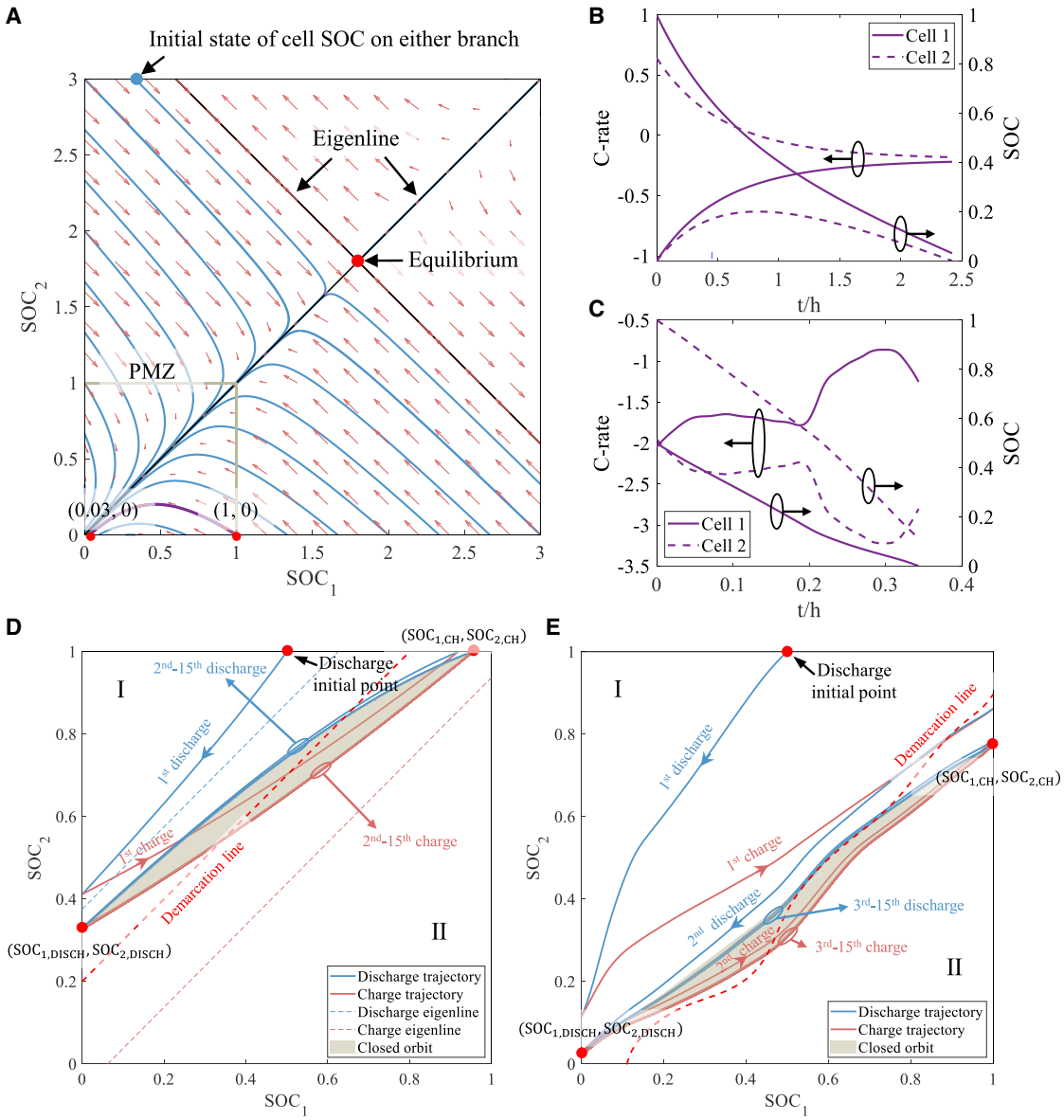

Figure 2. The phase-plane portrait and closed orbits of two-cell parallel systems

(A) The phase-plane portrait of two cells with the same simplified linear parameters for illustration: E-SOC = kSOC + b and R-SOC = mSOC + n. Average discharge C-rate on the branch is 0.2 C. The orthogonal decomposition of red arrows gives (i_1/C_1, i_2/C_2), where i_i and C_i are, respectively, current and capacity of the i cell (i = 1, 2).

(B) C-rate and SOC of two cells corresponding to the violet trajectory in (A). Discharge initial point is (1, 0).

(C) C-rate and SOC of two cells corresponding to the first discharge process in (E).

(D) The closed orbit in the phase-plane portrait during 15 charge/discharge cycles in a parallel system with linear parameters. Assume that the two cells have $C_1 = C_2$, E_1-SOC = k_1SOC$_1$ + b_1, E_2-SOC = k_2SOC$_2$ + b_2, R_1-SOC = m_1SOC$_1$ + n_1, and R_2-SOC = m_2SOC$_2$ + n_2. Average charge/discharge C-rate on the branch is 0.5 C. Discharge initial point is (0.5, 1).

(E) The closed orbit in the phase plane portrait during 15 charge/discharge cycles of a parallel system with NCA cathode with discharge initial point (0.5, 1) (parameters in Figure 3A). For illustration, assume that the E-SOC of cell 2 is 0.1 V larger than cell 1. Average charge/discharge C-rate on the branch is 2 C. ($SOC_{1,\ CH}$, $SOC_{2,\ CH}$) and ($SOC_{1,\ DISCH}$, $SOC_{2,\ DISCH}$) are the terminals of closed orbits. Blue solid curves are discharge trajectories, while red solid curves are charge trajectories. The red dotted lines are DLs.

equilibrium at the intersection of eigenlines, which determines the trajectory movements around it, always exceeds the boundary of PMZ (Note S3). It implies that linearizing the system near the equilibrium is not feasible, thus rendering classical

methods in linear system analysis inapplicable. Figure 2C gives an example of oscillating current, which corresponds to the first discharge process in Figure 2E. The phase-plane method helps present the time evolution of oscillations in the phase diagram and enables us to analyze the long-term pattern of parallel systems during repeated cycles.

By observing long-term behaviors during numerous repeated cycles of charging and discharging, we find that charge/discharge trajectories ultimately converge to a certain fixed region, a "closed orbit" in the SOC phase plane (gray parts in Figures 2D and 2E). The mathematical proof of the existence of a unique closed orbit is achieved for two-cell parallel systems. The closed orbit, present in almost all cases, is unique and unaffected by initial values. We will discuss some exceptions in the next section. To complete a general proof requires two steps.

The existence of a closed orbit can be proved by the demarcation line (step 1). Mathematical details can be found in Note S3, and here we only explain the main findings. The PMZ could be divided by the demarcation line $\Delta E = 0$ (DL) (red dotted lines in Figures 2D and 2E) into two parts (I and II in Figures 2D and 2E) with opposite convergence directions. In region I, trajectories converge to the DL from the upper part of it during the discharge/charge cycles. On the contrary, trajectories converge to the DL from the lower part of it in region II. Driven by these two opposing "forces," the moving trajectories will converge infinitely to a stationary state after some cycles since trajectories of the same process cannot overlap with each other, and the closed orbit will form in the phase plane. Obviously, the closed orbit must intersect with the DL, otherwise it never stops. The mathematical proof of the existence of a closed orbit is applicable to nonconstant current and different charging and discharging currents.

The uniqueness of a closed orbit can be proved by the Poincaré mapping method (step 2). Details can be found in Note S4. For any two initial points evolving to two endpoints after one charge and one discharge, endpoints are the Poincaré mapping of initial points (see Note S5 for more details). According to the nonintersecting property of trajectories of the same process, the distance between endpoints is smaller than that of initial points in all representative cases proposed based on the relative position of the closed orbit and the DL. Hence, the Poincaré mapping is a compression mapping according to Banach fixed-point theorem,[33] which proves the uniqueness of the closed orbit. The mathematical proof is applicable to nonconstant current and different charging and discharging currents on the condition that the repeated cycles are identical to each other.

Many numerical experiments of two-cell parallel systems have been performed to verify the preceding conclusions, with variables including common C-rate (0.04 C–10 C), resistance *R*-SOC (0%–25%), and capacity *C* (0%–9%), which are typical cell-to-cell variations from initial manufacture.[13] To the best of our knowledge, no analysis of the *E*-SOC variation has been provided in previous literature, probably due to its relative insensitivity to temperature and aging. Despite this, we still examined the 0%–10% *E*-SOC inconsistency to draw a sound conclusion. Parameters used in the simulation are from real cells with two types of cathode materials, including phase-change material lithium iron phosphate $LiFePO_4$(LFP) with flat *E*-SOC curves and solid solution material lithium nickel cobalt aluminium oxide $LiNi_{0.8}Co_{0.15}Al_{0.05}O2$(NCA) with steeper *E*-SOC curves (Figure 3). All experiments (48 in total) show that trajectories converge to form a stable and unique closed orbit after no more than 30 cycles (Figures S6–S13) and that all closed orbits intersect with the DL.

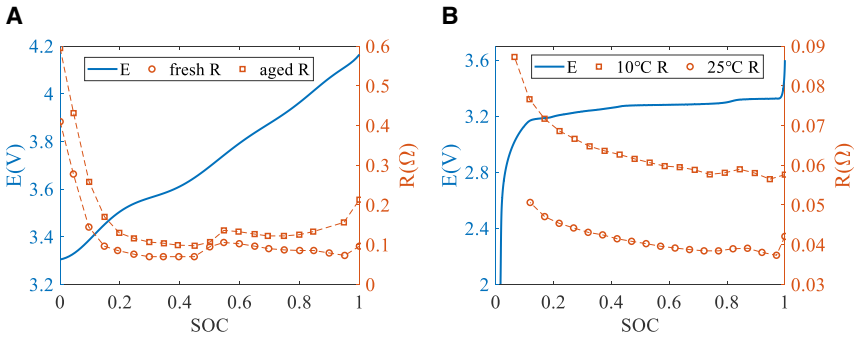

Figure 3. Open-circuit voltage *E*-SOC and resistance *R*-SOC curves of two actual parallel systems with two common types of cathode materials

(A) Solid solution material NCA. Parameters are taken from our previous research.[22] Cell 1 and cell 2 are fresh and aged, respectively. The capacity of each cell is 2.9463 and 2.7533 Ah, respectively.

(B) Phase-change material LFP (see experimental procedures for parameters determination). Cell 1 and cell 2 are set to 10°C and 25°C, respectively. The capacities of cell 1 and cell 2 are 2.8307 and 2.9402 Ah, respectively.

In conclusion, cycling trajectories converge toward the DL and are bound to stop around it in two-cell parallel systems. For multi-cell parallel systems, the demarcation curve still exists, arousing our speculation that closed orbits also exist. Nevertheless, due to the complex high-dimensional dynamic system, it is difficult to obtain the mathematical proof. Here, we adopt a compromise approach based on the conclusion of two-cell systems. Because the laminated cell is composed of electrode pairs connected in parallel internally, any parallel cells can be regarded as a single group with one *E*-SOC and *R*-SOC curve. In multi-cell parallel systems, cells can be divided into two groups. For this general parallel system consisting of two cell groups, the closed orbit exists and therefore the current flowing through each group varies periodically with the repeated cycles. We apply the same procedure for each group several times until each group only has one cell. It is concluded that the current through each cell varies periodically with the repeated cycles, indicating the existence of a unique closed orbit for the multi-cell parallel system.

Risks hiding behind stability

The first risk is the inevitable sacrifice of capacity utilization. For a single cell, it is well accepted that slow kinetics of mass transport and electrochemical reaction result in the loss of the available energy extracted from the cell before reaching the cutoff voltage. Parallel battery systems are found to inflict another intrinsic energy loss due to the inconsistency between cells on different branches. The residual SOC on either branch (as in Figures 2D and 2E) leads to an incomplete utilization of internal charge storage in the active material, thus reducing the actual Wh/kg or Wh/L of systems and wasting tremendous efforts made by materials scientists on improving the thermodynamic capability of battery materials, i.e., capacity density (mAh/g) and voltage. The position of the closed orbit in the phase portrait could help calibrate the loss. According to the terminals of the closed orbit, the capacity utilization of parallel systems can be evaluated as $\eta = \frac{\sum_{i=1}^{n}(SOC_{i,\ CH} - SOC_{i,\ DISCH})C_i}{\sum_{i=1}^{n} C_i}$, where n is the number of cells and ($SOC_{1,\ CH}$,…, $SOC_{i,\ CH}$) and ($SOC_{1,\ DISCH}$,…, $SOC_{i,\ DISCH}$) are the terminals of closed orbits. For example, the capacity utilization rates of the parallel system in Figures 2D and 2E are 81.29% and 88%, respectively. In contrast, when each cell is charged and discharged individually at half of the current, the capacity utilization is theoretically 100% when polarization is neglected. Notably, the capacity

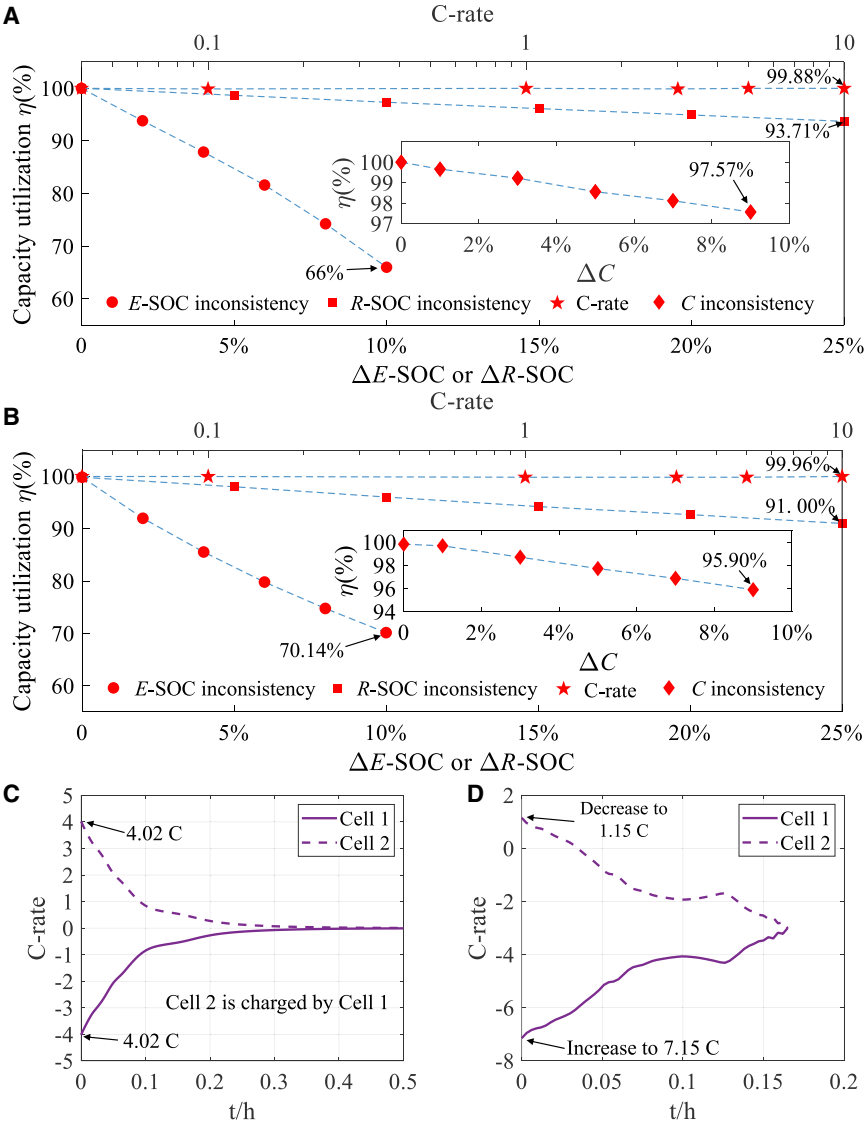

Figure 4. Risks of capacity loss and current overload in parallel systems

(A and B) Capacity utilization with inconsistencies in *C*, *E*-SOC, *R*-SOC, and charge/discharge C-rate of NCA cathode (A) and LFP cathode (B). Parameters are shown in Figure 3. Cell 1 is chosen as the baseline. Average charge/discharge C-rate on the branch is 2 C for the study of inconsistencies in *C*, *E*-SOC, and *R*-SOC.

(C) Cell currents of the parallel system with two large-format cells during the CB process.

(D) Cell currents of the same parallel system as (C) after applying a 6 C discharge current on the main circuit loop.

redistributes owing to the *E* difference between cells after cycles, but this process does not affect capacity utilization.

Inconsistencies in *C*, *E*-SOC, *R*-SOC, and current magnitude all affect the position and shape of the phase-plane portrait and, therefore, impact capacity utilization. Numerical experiments in the previous section are used to analyze the sensitivity of capacity utilization to these factors. Compared with the other three factors, current magnitude has a minor impact on capacity utilization (Figures 4A and 4B), which echoes the findings of Hosseinzadeh et al.[13] We infer that it is because the current

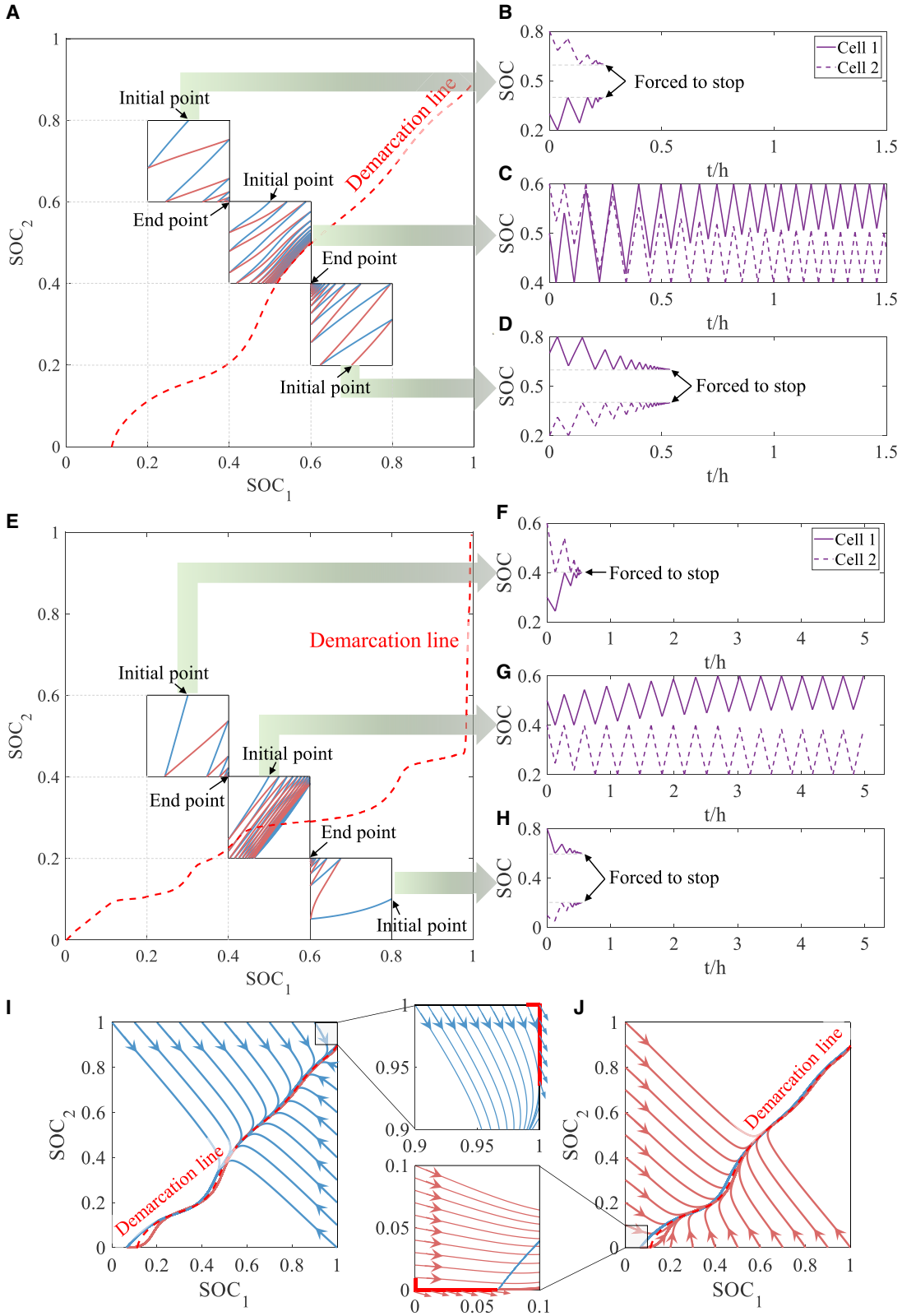
A
B
C
D
E
F
G
H
I
J
Initial point
End point
Demarcation line
Forced to stop
Cell 1
Cell 2
SOC
t/h
SOC1
SOC2

Figure 5. Risks of malfunctions in particular usage scenarios

(A–H) The malfunction risk of scenarios when cells cycle in a partial SOC range that does not intersect with the DL. Parameters are shown in Figure 3.

(A) Three SOC intervals in the phase plane portrait of NCA cathode during charge/discharge cycles. For illustration, assume that the *E*-SOC of cell 2 is 0.1 V larger than that of cell 1. Average charge/discharge C-rate on the branch is 3 C.

(B–D) The time evolution of SOC corresponding to three intervals in (A).

(E) Three SOC intervals in the phase-plane portrait of the LFP cathode during charge/discharge cycles. Assume that the *E*-SOC of cell 2 is 0.05 V larger than that of cell 1. Average charge/discharge C-rate on the branch is 1 C.

(F–H) The time evolution of SOC corresponding to three intervals in (E).

(I and J) The initial cell state remains unchanged at the corner of the PMZ (red boundary in insets of I and J) during two charge/discharge cycles. The first process is discharging (I) and charging (J), respectively. Average C-rate on the branch is 0.04 C.

magnitude does not affect current sharing and the DL that determines the position of closed orbits. In contrast, *E*-SOC inconsistency entails significant capacity waste with a waste rate reaching up to 34% (Figure 4A).

Another risk is possible current overload in the cell-balancing process. Replacement of cells in maintenance or repair of parallel systems happens frequently. After cell replacement, the system undergoes a cell-balancing (CB) process, indicating some cells being charged by others. In two-cell parallel systems, the corresponding trajectories have the negative slope in the phase-plane portrait. The CB current in every branch can be derived according to Kirchhoff's laws (Note S6), which is proportional to *E* difference and inversely proportional to resistance *R*. Therefore, parallel systems composed of large-format laminated cells (with more parallel electrode pairs inside leading to smaller *R*) have a higher CB current during the CB process. Two identical 20 Ah large-format lithium-ion cells with resistance on the order of magnitudes 1 mΩ are assumed to form a parallel system (parameters obtained from Ouyang et al.[34]). When the *E* difference is 554.3 mV with the initial point (0.8, 0.2), the transient CB current is estimated as 4.02 C (Figure 4C). If the parallel system functions and supplies energy to an external circuit during the CB process, the charging current on one branch will decrease, while the discharging current on another branch will increase (Figure 4D). Thus, the main circuit current should not be large enough to cause severe current overload on a certain branch, an unfavorable scenario for system safety, which could even result in a blown fuse. A well-established solution to address the aforementioned risk is to reduce the *E* difference, such as by pre-discharging/pre-charging the swapping cell or installing switches on the branches to control individual cells.

Malfunctions may occur in particular usage scenarios. We have proven that the cycling trajectories converge toward the DL during repeated cycles in a full SOC range with SOC either reaching 0 on the left or bottom part or reaching 1 on the right or top part of the PMZ. This rule may lead to malfunctions in scenarios when cells cycle in a partial SOC range that does not intersect with the DL. For example, in SOC ranges corresponding to Figures 5B, 5D, 5F, and 5H, the cycling trajectories move in a certain direction, and the cell will ultimately be in a fixed state, indicating that either charging or discharging is forced to stop. In contrast, in the SOC zone that intersects with the DL, such as in Figures 5C and 5G, the parallel systems function well, and the closed orbit appears in this partial zone. The above discussion is based on arbitrary SOC states. In general, when cells are connected in parallel, their voltages tend to be the same. Therefore, the cell states will be on the DL after the CB process.

Another malfunction scenario is that the initial cell state remains unchanged at the corner of the PMZ (red boundary in insets of Figures 5I and 5J) and needs a

powerful enough current to "drag it out". At the red boundary, the trajectory slope is negative so that the parallel system cannot discharge/charge due to the boundary constraint. As mentioned in the last subsection, the negative trajectory slope indicates one cell being charged by the other. However, at the red boundary in Figure 5I, cell 1 with a full SOC cannot be charged by cell 2. Similarly, cell 2 with an empty SOC cannot charge cell 1 at the red boundary in Figure 4J. To fix this malfunction, a powerful enough current, which is larger than the CB current boundary, should be applied to restore a positive trajectory slope. The CB current boundary can be derived from Kirchhoff's laws (Note S6), which are $\sum_{i=1}^{n} \frac{E_i - E_{\text{lowest } E}}{R_i}$ and $\sum_{i=1}^{n} \frac{E_{\text{highest } E} - E_i}{R_i}$ for the discharge and charge processes, respectively. Parallel systems without the *E*-SOC inconsistency can work well even with the negative trajectory slope.

In summary, the parallel battery configuration generates inherent self-excited oscillation without requiring any external oscillating excitation, which raises concerns about stability within parallel battery systems. We show the parallel battery system to be essentially a convergent, stable, and robust system with a highly precise and absolutely reliable battery management system. The long-term trajectory of batteries connected in parallel in repeated cycles will be enveloped in a closed orbit insensitive to initial states of systems. In an era of rapidly developing renewable energy and large-scale battery systems, the completion of this proof is reassuring and has enormous significance: the parallel configuration, inevitable for a large-scale BESS, is intrinsically safe, which lays the groundwork for building a large-scale BESS. We also remind all in the industry to beware of risks arising from parallel configuration: inevitable capacity loss, possible current overload, and accidental malfunctions.

EXPERIMENTAL PROCEDURES

Resource availability

Lead contact

Further information and requests for resources and reagents should be directed to and will be fulfilled by the lead contact, Zhe Li (zhe_li@tsinghua.edu.cn).

Materials availability

This study did not generate new unique reagents.

Data and code availability

All data supporting the results of this study are available within the article and supplemental information. This study does not report original code. Any additional information required to reanalyze the data reported in this article is available from the lead contact upon reasonable request.

Definition of *Net Zero* as a broad motivation

Net zero is defined assuming that a significant tightening of climate policies leads to a pronounced and sustained fall in CO_2-equivalent (CO_{2e}) emissions. The fall in emissions is aided by a shift in societal behavior and preferences that further support gains in energy efficiency and the adoption of low-carbon energy sources. CO_{2e} emissions fall by around 95% by 2050 (relative to 2019 levels). The pace and extent of this fall is broadly consistent with scenario of "limit the global average temperature increase to 1.5°C above pre-industrial levels by 2100."[1]

Actual tests of a two-cell parallel system with LFP cathode

We parallel connected two Sony 26650 cells with an LFP-based positive electrode and measured the current on each branch. The difficulties of this seemingly easy experiment are to (1) minimize the contact resistance on wires and welding nodes and (2) generate a stable and controllable temperature gradient between two cells. To reach these goals, we designed a special test bench, as shown in Figure S1. Details about the test bench can be found in other publications.[35,36] To minimize the contact resistance, a shunt current transducer with resistance of 1.0 mΩ was employed. The electrical connection between the cell and the shunt current transducer was shown in Figures S1B and S1C. The external resistance in one string is about 1.3 mΩ, which is smaller than the cell resistance. The temperature control unit consists of Peltier elements with proportional-integral-derivative (PID) control and copper shells. A control sensor and a measuring sensor were put in a 10 mm depth hole of the copper shell next to the positive connector and the negative connector, respectively. A highly precise temperature sensor showed that the difference between measuring points is less than 0.2°C.

Cell 1 and cell 2 are set to 10°C and 25°C, respectively. The simulated and experimental C-rate and SOC on each branch are shown in Figures S1D and S1E. They represent good agreement except for the low SOC region using the extrapolation of the internal resistance.

Parameters determination of Sony 26650 cells with LFP-based positive electrode

Three sets of parameters, that is, capacity, open-circuit voltage *E*-SOC curve, and resistance *R*-SOC curve, are required for the Rint battery model. The determination methods are listed below:

(1) Capacity was measured by two steps: (1) constant current constant voltage (CCCV) charge with a CC rate of 0.5 C and a cutoff current of 0.1 C at 3.6 V, then (2) $^1/_3$C discharge to 2.0 V.
(2) Resistance was determined by the current interrupt method at 5% SOC intervals, involving discharging the cell with a current of 1 C for 18 s, followed by a 2 h relaxation process. The resistance was calculated by $R = (V_1 - V_2)/I$, where I is the interrupting current, and V_1 and V_2 are the cell voltage before and after the current interrupt, respectively.
(3) The cell voltage at the end of the relaxation process was adopted as E.

The capacities of cell 1 and cell 2 are 2.8307 and 2.9402 Ah, respectively. *E*-SOC and *R*-SOC curves are shown in Figure 3.

SUPPLEMENTAL INFORMATION

Supplemental information can be found online at https://doi.org/10.1016/j.xcrp.2022.101154.

ACKNOWLEDGMENTS

This work is supported by the National Natural Science Foundation of China under grant number U1864214 and the National Key Research and Development Program of China under grant number 2021YFB2401800.

AUTHOR CONTRIBUTIONS

Z.L. and J.Z. conceived the idea. Z.L. designed the experiments with support from M.H.H. A.J. supervised the experiments. A.Z. and Z.M. conducted data analysis.

M.L. and A.Z. conceived the mathematical proof. A.Z., Z.M., and C.W. performed all simulations. Z.L., A.Z., Z.M., M.L., and J.Z. discussed the results and commented on the manuscript. A.Z. and Z.L. wrote the manuscript with input from all co-authors.

DECLARATION OF INTERESTS

The authors declare no competing interests.

Received: August 24, 2022
Revised: September 29, 2022
Accepted: November 1, 2022
Published: November 22, 2022

REFERENCES

1. BP. (2022). Energy Outlook, 2022 Edition (BP).
2. BloombergNEF. (2021). Global Energy Storage Outlook (BloombergNEF).
3. Kimoto, T. (2015). Material science and device physics in SiC technology for high-voltage power devices. Jpn. J. Appl. Phys. *54*, 040103.
4. Kasap, S.O., and Capper, P. (2017). Springer Handbook of Electronic and Photonic Materials (Springer).
5. Pastor-Fernández, C., Bruen, T., Widanage, W., Gama-Valdez, M., and Marco, J. (2016). A study of cell-to-cell interactions and degradation in parallel strings: implications for the battery management system. J. Power Sources *329*, 574–585.
6. Colthorpe, A. (2021). Energy Storage News. *Huawei signs 1,300MWh solar-charged Battery Contract for Saudi Arabia's Red Sea Project* (Energy Storage NEWS).
7. Spurrett, R., Thwaite, C., Holland, A., Lizius, D., and Dudley, G. (2002). Modeling of Highly-Parallel Lithium-Ion Batteries (Space Power, Proceedings of the Sixth European Conference held 6-10 May, 2002 in Porto, Portugal. European Space Agency), pp. 685–691.
8. Wu, M.-S., Lin, C.-Y., Wang, Y.-Y., Wan, C.-C., and Yang, C.R. (2006). Numerical simulation for the discharge behaviors of batteries in series and/or parallel-connected battery pack. Electrochim. Acta *52*, 1349–1357. https://doi.org/10.1016/j.electacta.2006.07.036.
9. Pastor-Fernandez, C., Bruen, T., Widanage, W.D., Gama-Valdez, M.A., and Marco, J. (2016). A study of cell-to-cell interactions and degradation in parallel strings: implications for the battery management system. J. Power Sources *329*, 574–585. https://doi.org/10.1016/j.jpowsour.2016.07.121.
10. Fill, A., Koch, S., Pott, A., and Birke, K.P. (2018). Current distribution of parallel-connected cells in dependence of cell resistance, capacity and number of parallel cells. J. Power Sources *407*, 147–152. https://doi.org/10.1016/j.jpowsour.2018.10.061.
11. Rumpf, K., Rheinfeld, A., Schindler, M., Keil, J., Schua, T., and Jossen, A. (2018). Influence of cell-to-cell variations on the inhomogeneity of lithium-ion battery modules. J. Electrochem. Soc. *165*, A2587–A2607. https://doi.org/10.1149/2.0111811jes.
12. Fill, A., Koch, S., and Birke, K.P. (2019). Analytical model of the current distribution of parallel-connected battery cells and strings. J. Energy Storage *23*, 37–43. https://doi.org/10.1016/j.est.2019.02.031.
13. Hosseinzadeh, E., Arias, S., Krishna, M., Worwood, D., Barai, A., Widanalage, D., and Marco, J. (2021). Quantifying cell-to-cell variations of a parallel battery module for different pack configurations. Appl. Energy *282*. https://doi.org/10.1016/j.apenergy.2020.115859.
14. Gogoana, R., Pinson, M.B., Bazant, M.Z., and Sarma, S.E. (2014). Internal resistance matching for parallel-connected lithium-ion cells and impacts on battery pack cycle life. J. Power Sources *252*, 8–13. https://doi.org/10.1016/j.jpowsour.2013.11.101.
15. Bruen, T., and Marco, J. (2016). Modelling and experimental evaluation of parallel connected lithium ion cells for an electric vehicle battery system. J. Power Sources *310*, 91–101. https://doi.org/10.1016/j.jpowsour.2016.01.001.
16. Liu, X.H., Ai, W.L., Marlow, M.N., Patel, Y., and Wu, B. (2019). The effect of cell-to-cell variations and thermal gradients on the performance and degradation of lithium-ion battery packs. Appl. Energy *248*, 489–499. https://doi.org/10.1016/j.apenergy.2019.04.108.
17. Fleckenstein, M., Bohlen, O., Roscher, M.A., and Baker, B. (2011). Current density and state of charge inhomogeneities in Li-ion battery cells with LiFePO4 as cathode material due to temperature gradients. J. Power Sources *196*, 4769–4778. https://doi.org/10.1016/j.jpowsour.2011.01.043.
18. Yang, N.X., Zhang, X.W., Shang, B.B., and Li, G.J. (2016). Unbalanced discharging and aging due to temperature differences among the cells in a lithium-ion battery pack with parallel combination. J. Power Sources *306*, 733–741. https://doi.org/10.1016/j.jpowsour.2015.12.079.
19. Zhang, Y., Zhao, R., Dubie, J., Jahns, T., and Juang, L. (2016). Investigation of Current Sharing and Heat Dissipation in Parallel-Connected Lithium-Ion Battery Packs, pp. 1–8.
20. Klein, M.P., and Park, J.W. (2017). Current distribution measurements in parallel-connected lithium-ion cylindrical cells under non-uniform temperature conditions. J. Electrochem. Soc. *164*, A1893–A1906. https://doi.org/10.1149/2.0011709jes.
21. Gong, X.Z., Xiong, R., and Mi, C.C. (2015). Study of the characteristics of battery packs in electric vehicles with parallel-connected lithium-ion battery cells. IEEE Trans. Ind. Appl. *51*, 1872–1879. https://doi.org/10.1109/Tia.2014.2345951.
22. An, F.Q., Huang, J., Wang, C.Y., Li, Z., Zhang, J.B., Wang, S., and Li, P. (2016). Cell sorting for parallel lithium-ion battery systems: evaluation based on an electric circuit model. J. Energy Storage *6*, 195–203. https://doi.org/10.1016/j.est.2016.04.007.
23. Miyatake, S., Susuki, Y., Hikihara, T., Itoh, S., and Tanaka, K. (2013). Discharge characteristics of multicell lithium-ion battery with nonuniform cells. J. Power Sources *241*, 736–743. https://doi.org/10.1016/j.jpowsour.2013.05.179.
24. Kamalisiahroudi, S., Huang, J., Li, Z., and Zhang, J. (2014). Study of temperature difference and current distribution in parallel-connected cells at low temperature. Int. J. Electr. Robot. Electron. Commun. Eng. *8*, 1589.
25. LeBel, F.A., Wilke, S., Schweitzer, B., Roux, M.A., Al-Hallaj, S., and Trovao, J.P.F. (2016). A Lithium-Ion Battery Electro-Thermal Model of Parallellized Cells (2016 IEEE 84th Vehicular Technology Conference (VTC-Fall)), pp. 1–6.
26. Baumann, M., Wildfeuer, L., Rohr, S., and Lienkamp, M. (2018). Parameter variations within Li-Ion battery packs – theoretical investigations and experimental quantification. J. Energy Storage *18*, 295–307. https://doi.org/10.1016/j.est.2018.04.031.
27. Grun, T., Stella, K., and Wollersheim, O. (2018). Influence of circuit design on load distribution and performance of parallel-connected Lithium ion cells for photovoltaic home storage systems. J. Energy Storage *17*, 367–382. https://doi.org/10.1016/j.est.2018.03.010.
28. Chang, L., Wang, C.Y., Zhang, C.H., Xiao, L.J., Cui, N.X., Li, H.Y., and Qiu, J.F. (2020). A novel fast capacity estimation method based on current curves of parallel-connected cells for retired lithium-ion batteries in second-use applications. J. Power Sources *459*, 227901. https://doi.org/10.1016/j.jpowsour.2020.227901.

29. Gabbar, H.A., Othman, A.M., and Abdussami, M.R. (2021). Review of battery management systems (BMS) development and industrial standards. Technologies *9*. https://doi.org/10.3390/technologies9020028.

30. Nikdel, M. (2014). Various battery models for various simulation studies and applications. Renew. Sustain. Energy Rev. *32*, 477–485. https://doi.org/10.1016/j.rser.2014.01.048.

31. Han, Z., Xu, N., Chen, H., Huang, Y., and Zhao, B. (2018). Energy-efficient control of electric vehicles based on linear quadratic regulator and phase plane analysis. Appl. Energy *213*, 639–657. https://doi.org/10.1016/j.apenergy.2017.09.006.

32. Kimoto, M., and Ghil, M. (1993). Multiple flow regimes in the Northern Hemisphere winter. Part I: methodology and hemispheric regimes. J. Atmos. Sci. *50*, 2625–2644.

33. Agarwal, P., Jleli, M., and Samet, B. (2018). Banach contraction principle and applications. In Fixed Point Theory in Metric Spaces: Recent Advances and Applications, P. Agarwal, M. Jleli, and B. Samet, eds. (Springer Singapore), pp. 1–23. https://doi.org/10.1007/978-981-13-2913-5_1.

34. Ouyang, M., Ren, D., Lu, L., Li, J., Feng, X., Han, X., and Liu, G. (2015). Overcharge-induced capacity fading analysis for large format lithium-ion batteries with Li Ni1/3Co1/3Mn1/3O2+ Li Mn2O4 composite cathode. J. Power Sources *279*, 626–635. https://doi.org/10.1016/j.jpowsour.2015.01.051.

35. Brand, M.J., Hofmann, M.H., Steinhardt, M., Schuster, S.F., and Jossen, A. (2016). Current distribution within parallel-connected battery cells. J. Power Sources *334*, 202–212. https://doi.org/10.1016/j.jpowsour.2016.10.010.

36. Jocher, P., Steinhardt, M., Ludwig, S., Schindler, M., Martin, J., and Jossen, A. (2021). A novel measurement technique for parallel-connected lithium-ion cells with controllable interconnection resistance. J. Power Sources *503*. https://doi.org/10.1016/j.jpowsour.2021.230030.